Two-Stage Hydrothermal Growth of Long ZnO Nanowires for Efficient TiO 2 Nanotube-Based Dye-Sensitized Solar Cells

ARTICLE *in* THE JOURNAL OF PHYSICAL CHEMISTRY C · MARCH 2012

Impact Factor: 4.77 · DOI: 10.1021/jp300960r

2 AUTHORS, INCLUDING:

Chengkun Xu
University of Pittsburgh
20 PUBLICATIONS **969** CITATIONS

THE JOURNAL OF PHYSICAL CHEMISTRY C

Article

pubs.acs.org/JPCC

Two-Stage Hydrothermal Growth of Long ZnO Nanowires for Efficient TiO_2 Nanotube-Based Dye-Sensitized Solar Cells

Chengkun Xu and Di Gao*

Department of Chemical and Petroleum Engineering, University of Pittsburgh, Pittsburgh, Pennsylvania 15261, United States

ABSTRACT: Vertically aligned TiO_2 1-D nanostructures synthesized directly on transparent conducting oxide (TCO) have shown great promise to overcome the limitation of the random network of TiO_2 nanoparticles currently used in dye-sensitized solar cells (DSCs). A promising process for synthesis of such structures is to first grow aligned ZnO nanowire arrays and then convert them to TiO_2 nanotubes. Growth of ZnO nanowires with a sufficient length and density but without fusion of their roots, however, remains challenging. In this paper, we investigate the dependence of wire density and aspect ratio on the temperature, concentrations of reagents, and seeding crystals used in a liquid-phase ZnO nanowire synthesis process. On the basis of the results of the investigation, we introduce a two-step hydrothermal process for synthesis of long and vertically aligned ZnO nanowire arrays, and demonstrate that, by dividing the wire growth process into two steps at two different temperatures and reducing Zn^{2+} concentration, ZnO nanowires up to 20 μm long can be obtained without fusing their roots. The resulting ZnO nanowires can be converted into TiO_2 nanotubes, and DSCs fabricated using such TiO_2 nanotubes yield power conversion efficiencies up to 6.1%.

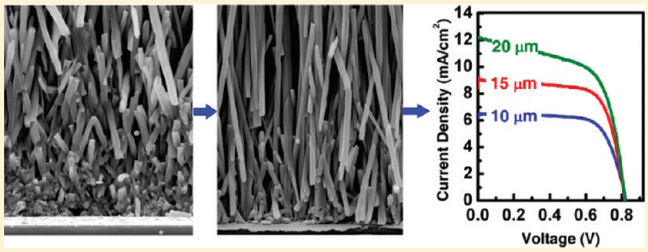

INTRODUCTION

Replacing the disordered TiO_2 mesoporous films that are currently used as anodes in dye-sensitized solar cells (DSCs) with vertically aligned nanostructures directly synthesized on transparent conductive oxides (TCO) has been identified as one of the most promising approaches for overcoming the technological limits of current DSCs.[1,2] Compared to the disordered mesoporous films, the vertically aligned nanostructures greatly promote electron transport and facilitate infiltration of solid or viscous chemicals (such as solid-state electrolytes, quantum dots, and ionic liquids) into the anodes. A number of DSCs with such anodes have been fabricated,[3−12] and significantly enhanced electron transport properties have been demonstrated.[13−17] However, the energy conversion efficiency of these DSCs is still considerably lower than that of their nanoparticle-based counterparts.[3−6,8,10,11] This is primarily due to the much lower internal surface area of the vertically aligned 1-D nanostructures compared to mesoporous films, which leads to insufficient dye adsorption and, therefore, low light harvesting efficiency. Apparently, this problem may be resolved by increasing either the aspect ratio or the density of the 1-D nanostructures, which nevertheless has been proven challenging in practice.

In our previous work, we have reported a liquid-phase conversion process for synthesizing TiO_2 nanotubes by using ZnO nanowire arrays as a template.[10] The TiO_2 nanotube synthesis process mainly consists of two steps: (i) growth of ZnO nanowire arrays and (ii) hydrothermal conversion of ZnO nanowires to TiO_2 nanotubes via TiO_2 deposition and simultaneous ZnO dissolution. We have demonstrated synthesis of TiO_2 nanotubes up to 10 μm long and fabrication of DSCs with efficiencies up to 3.6% through this approach.[10] However, further improvement of such DSCs has been difficult because of our limited capability in synthesizing long ZnO nanowires. Although we have developed a wet chemical process for growth of ZnO nanowires up to 40 μm long,[11] such long wires are typically fused at their root and, as a result, a significant percentage of the surface area gained by increasing the wire length is lost. This problem becomes more significant when the ZnO nanowires are converted to TiO_2 nanotubes, during which the diameter of the nanostructure slightly increases. Most recently, we have developed a process to synthesize multilayer assemblies of ZnO nanowire arrays which addresses the wire fusion problem.[18] The capability of the multilayer assembling method will be further enhanced if we are able to synthesize long and nonfusing ZnO nanowire arrays for each layer.

In this paper, we first investigate how the process parameters, particularly the temperature, the density of seed crystals, and the concentration of reactants used in the liquid-phase ZnO nanowire array synthesis process, affect the density and aspect ratio of the wires. On the basis of the results of the investigation, we introduce a two-stage hydrothermal process for growth of vertically aligned long ZnO nanowires. We demonstrate that, by dividing the wire growth process into two steps at two different temperatures and reducing the Zn^{2+} concentration, ZnO nanowires up to 20 μm long can be obtained without fusing their roots. The resulting wires can be

Received: January 30, 2012
Revised: March 7, 2012
Published: March 8, 2012

   dx.doi.org/10.1021/jp300960r | J. Phys. Chem. C 2012, 116, 7236−7241

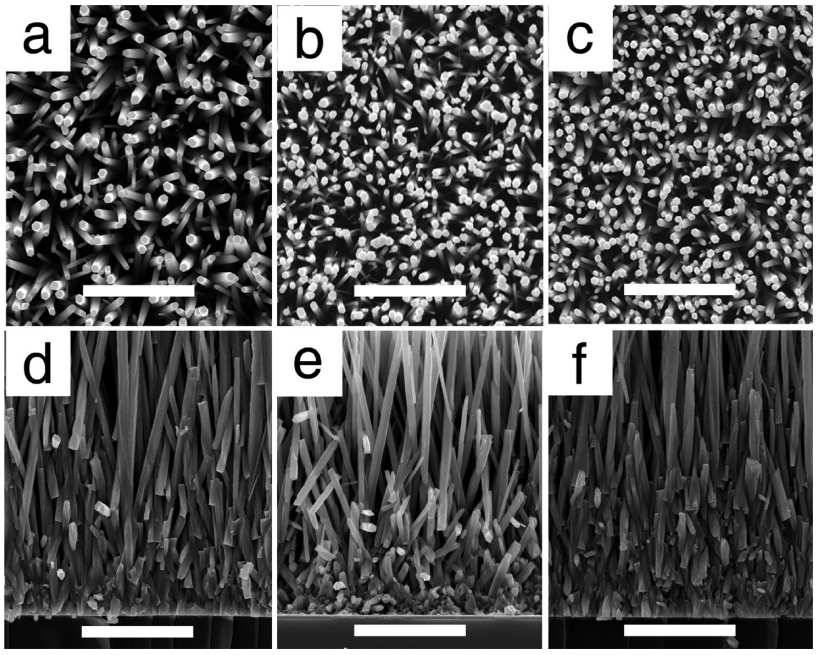

Figure 1. Top-view (a, b, and c) and side-view (d, e, and f) SEM images of ZnO nanowire arrays synthesized at different temperatures. The growth solution consists of 25 mM $Zn(NO_3)_2$ + 12.5 mM HMTA + 0.25 M NH_4OH + 2 mM PEI. The substrates are seeded using 2 mM seeding solution. The bath temperature is kept at (a and d) 85 °C, (b and e) 88 °C, and (c and f) 90 °C, respectively. Scale bar, 5 μm.

converted to vertically aligned TiO_2 nanotubes up to 20 μm long. DSCs fabricated using arrays of such long TiO_2 nanotubes yield power conversion efficiencies up to 6.1%, which is comparable to TiO_2 nanoparticle-based DSCs.

EXPERIMENTAL SECTION

Synthesis of ZnO Nanowire Arrays on TCO. ZnO nanowire arrays were grown on indium doped tin oxide (ITO) glass substrates. The substrates were first cleaned by acetone/ethanol sonication/UVO and deposited with a layer of TiO_2 of thickness ~30 nm by immersing the substrate in a solution of 0.1 M $(NH_4)_2TiF_6$ + 0.2 M H_3BO_3 for 30 min at 25 °C. The substrates were then seeded by spin coating with zinc acetate solution in ethanol at a speed of 500 rpm, followed by thermal decomposition at 300 °C for 20 min. The concentration of the zinc acetate solution was varied from 1 to 5 mM for investigating the effect of the seed crystal density on the nanowire growth. For all other experiments described in this paper, 2 mM zinc acetate solution was used for deposition of the seed layer. The seeded substrates are placed in an aqueous solution containing 7.5−25 mM zinc nitrate, 3.75−12.5 mM hexamethylenetetramine (HMTA), 2 mM polyethylenimine (PEI), and 0.15−0.25 M ammonium hydroxide. The temperature of the chemical bath was varied from 85 to 90 °C to investigate the effect of temperature on the nanowire growth. For the two-stage growth of long ZnO nanowires, the temperature of the solution was kept first at 88−89 °C for 10 min and then at 85 °C for 12 h.

Conversion of ZnO Nanowires to TiO_2 Nanotubes. The synthesized ZnO nanowire arrays on ITO were immersed in an aqueous solution consisting of 0.075 M $(NH_4)_2TiF_6$ and 0.2 M H_3BO_3 at room temperature for 0.5 h. In this solution, $(NH_4)_2TiF_6$ hydrolyzed to TiO_2 on the surface of individual ZnO nanowires, while ZnO dissolved simultaneously in the solution with acids produced by $(NH_4)_2TiF_6$ hydrolysis. The resulting array of TiO_2 nanotubes, which were top-end closed, was then dipped in a glycerol solution containing 3 wt % HF and 12 wt % water for 2 min to etch away the top-end of the array, followed by immersing in a 0.5 M H_3BO_3 solution for 2 h to remove any residual ZnO inside the tubes. Glycerol in the etching solution acted to increase the solution viscosity and therefore slowed down the infiltration rate of the solution into the nanotube arrays. By choosing appropriate concentrations of HF and glycerol and dipping time, only an about 1 μm long section of each tube was etched away from the top, resulting in tubes with an open end. The arrays were rinsed with DI water and calcined in air at 450 °C for 30 min to further increase crystallinity.[19,20]

Fabrication and Characterization of DSCs. The synthesized TiO_2 nanotubes were immersed in 0.5 mM $(Bu_4N)_2[Ru(4,4'\text{-}(COOH)\text{-}2,2,\text{-bipyridine})_2(NCS)_2]$ (N719 dye) in 1:1 acetonitrile/tert-butyl alcohol overnight. A 60 μm thick hot melt sealing foil (SX1162-60, Solaronix) frame was sandwiched between the sensitized films and a platinized ITO electrode. A solution consisting of 0.1 M LiI, 0.1 M I_2, 0.5 M tert-butylpyridine, and 0.6 M tetrabutylammonium iodide in acetonitrile was introduced into the cell. Cells were immediately tested under AM 1.5G simulated sunlight (model 67005, Oriel) using a Reference 600 Potentiostat (Gamry Instruments). Monochromatic illumination was achieved through an M 77250 monochromator (Oriel). Incident photon-to-current efficiencies (IPCE) were measured with the same potentiostat. Active areas were limited to about 0.2 cm^2 by the sealing frame.

RESULTS AND DISCUSSION

Dependence of the Density and Aspect Ratio of ZnO Nanowires on the Growth Temperature. We first investigated how the growth temperature affects the ZnO nanowire density and aspect ratio. Parts a, b, and c of Figure 1 show top-view scanning electron microscopy (SEM) images of ZnO nanowire arrays synthesized at chemical bath temper-

dx.doi.org/10.1021/jp300960r | J. Phys. Chem. C 2012, 116, 7236−7241

atures of 85, 88, and 90 °C, respectively. Parts d, e, and f of Figure 1 are side-views of the lower portion of the arrays shown in parts a, b, and c, respectively. The seeding layer for these arrays was prepared by the same method, i.e., by spin-coating 2 mM zinc acetate solution in ethanol followed by thermal decomposition at 300 °C for 20 min. The thickness of all these three nanowire arrays is about 15 μm. The average density, diameter, and aspect ratio (calculated from the average length and diameter) of the wires in each array are summarized in Table 1. It is found that the wire density considerably increases with the bath temperature. A plausible explanation is provided as the following. Prior to the growth of ZnO nanowire arrays, the size of ZnO seed nanocrystals ranges from 3 to 20 nm.[21] At the initial stage, the growth rate of different sized nanocrystals varies depending on their supersaturation, which is a function of the crystal size because of the size-dependent solubility of small crystals. The relationship between the crystal size (r) and the solubility (c) can be described by the Ostwald–Freundlich equation:[22]

Table 1. The Densities, Diameters, and Aspect Ratios of Wires Grown at Different Temperatures as Shown in Figure 1a–c

	temperature (°C)	wire density (10^8/cm^2)	wire diameter (nm)	wire aspect ratio
Figure 1a	85	4.7	362 ± 56	41
Figure 1b	88	8.1	260 ± 73	61
Figure 1c	90	9.5	322 ± 51	48

$$\ln\left[\frac{c(r)}{c_0}\right] = \frac{\gamma \cdot \Omega}{r k_B T} \quad (1)$$

where $c(r)$ is the solubility of small crystals of radius r, c_0 is the solubility of bulk crystal, Ω is the molecular volume, γ is the surface free energy, T is the temperature, and k_B is the Boltzmann constant. According to eq 1, in the same chemical bath, smaller seeds will have a larger solubility and be at lower supersaturation than larger seeds. Thus, smaller seeds will grow at a lower rate than the larger ones. However, such a size effect on the nanocrystal growth is only significant when the nanocrystals are smaller than a certain critical size. Above the critical size, the crystals will grow at approximately the same rate. With a certain set of process parameters, only those seed nanocrystals that can grow to a critical size at the initial stage (before the mass transport becomes the limiting factor for the growth of nanowires at the lower portion of the arrays) will eventually grow into wires that reach the top of the array. A higher chemical bath temperature favors a faster growth rate for all seed nanocrystals at the initial stage, and therefore, more seed nanocrystals will have the opportunity to reach the critical size required for them to grow into wires that can reach the top of the array, which leads to a denser nanowire array.

Different from the monotonic increase trend observed for the wire density, the wire diameter is seen to first decrease and then increase as temperature increases. This is likely because that the wire diameter is determined by the lateral growth rate of the wires, while the latter is affected by both the bath temperature and the wire density. Higher temperature favors the chemical reaction and deposition of ZnO, but it also leads to a denser array which makes the deposition of ZnO on the sidewall of the nanowires more limited by mass transfer. As the growth temperature increases from 85 to 88 and then to 90 °C, the effect of mass transfer limitation first dominates and then the favor of higher temperatures on higher chemical reaction rates dominates and, consequently, the wire diameter is seen to decrease first and then increase.

Despite the difference in their density and diameter, the wires grown at these three different temperatures have a common feature—they are all fused at their root to some extent. Relatively speaking, at lower temperatures, the density of wires is smaller, but the wires, especially their bottom portion, tend to grow wider because of less limitation of mass transfer of reactants, which is the primary reason for fusion of wires at such temperatures. At higher temperatures, the density of wires is larger and the wires are thinner, but another factor comes into play—the formation of short wires between the roots of the long ones. This is clearly seen in Figure 1e and f, which is responsible for fusion of wires at these two temperatures. While short wires are also observed in Figure 1d, they are a less important factor compared to the widening of wires for causing the wire fusion at this temperature. The formation of short wires is primarily caused by the size-dependent growth of the seed crystals. Those small seed nanocrystals will grow at a much lower rate than the wires and eventually fuse the roots of long wires. Higher growth temperature favors the growth of these small seed crystals, and therefore, formation of short wires becomes more significant at higher growth temperatures.

Dependence of the Density and Aspect Ratio of ZnO Nanowires on the Seeding Solution Concentration. As discussed above, high wire density may cause wire fusion at their root. To avoid "crowding" of wires at their root, the first approach that comes to mind is probably reducing the seed density on substrates by lowering the concentration of the seeding solution. Figure 2 shows SEM images of ZnO nanowire arrays synthesized using different seeding solution concen-

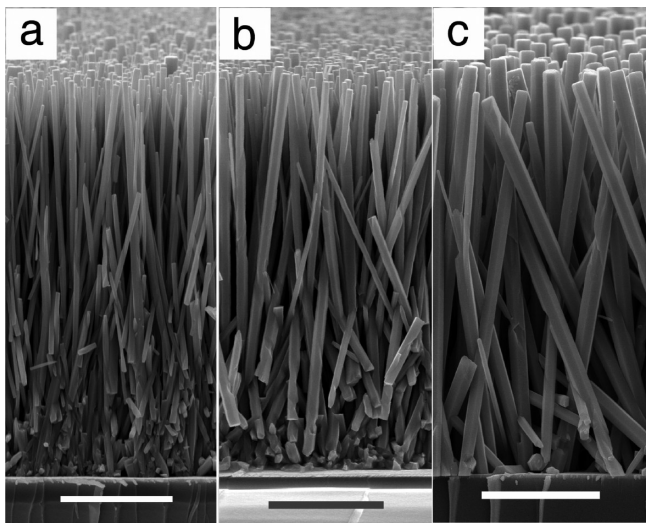

Figure 2. SEM images of ZnO nanowire arrays synthesized using different seeding solution concentrations. The growth solution consists of 25 mM $Zn(NO_3)_2$ + 12.5 mM HMTA + 0.25 M NH_4OH + 2 mM PEI. The bath temperature is 88 °C. The substrates are seeded by using (a) 5 mM, (b) 2 mM, and (c) 1 mM seeding solutions, respectively. Scale bar, 5 μm.

dx.doi.org/10.1021/jp300960r | J. Phys. Chem. C 2012, 116, 7236–7241

trations. The wires in Figure 2a, b, and c are synthesized in 25 mM Zn^{2+} solution at 88 °C with seed layers formed from 5, 2, and 1 mM $Zn(CH_3COO)_2$ seeding solutions, respectively. The wire densities, diameters, and aspect ratios of the arrays are summarized in Table 2. Wires in Figure 2a, synthesized using

Table 2. The Densities, Diameters, and Aspect Ratios of Wires Shown in Figure 2[a]

	concentration of seeding solution (mM)	wire density (10^8/cm^2)	wire diameter (nm)	wire aspect ratio
Figure 2a	5	11.4	170 ± 60	113
Figure 2b	2	7.7	315 ± 87	58
Figure 2c	1	2.6	585 ± 80	30

[a]These wires are grown from different seed layers formed by using different seeding solution concentrations.

the highest seeding solution concentration, exhibit the highest wire density and aspect ratio, but they are fused at their root. It is not surprising that lowering the concentration of the seeding solution decreases the wire density and alleviates the wire fusion problem. Such an effect can be seen when the concentration of the $Zn(CH_3COO)_2$ seeding solution is reduced from 5 to 2 mM (Figure 2b), and it becomes more obvious when the seeding solution concentration is further reduced to 1 mM (Figure 2c). However, reducing the wire density also leads to loss of surface areas. For example, in comparison to the nanowire array shown in Figure 2b, the nanowire array shown in Figure 2c has a lot less wire fusion problems, but more surface area is lost due to the decrease of the wire density than the surface area gained by the effort of avoiding the wire fusion. Therefore, the approach of lowering seeding solution concentrations to alleviating the wire fusion problem can only be taken moderately.

Two-Stage Hydrothermal Growth of ZnO Nanowire Arrays. On the basis of the above results and discussion, it can be seen that, in order to obtain arrays of long ZnO nanowires without fusing their roots, three problems need to be addressed: wire density, wire widening, and formation of short wires between the long ones. The wire density can be controlled by using appropriate seeding solution concentrations for a certain growth temperature. To address the short wire formation and wire widening problems, we have taken two approaches. Given that the formation of short wires is mainly a result of the size-dependent growth of the seed nanocrystals, in order to suppress it, our first approach is to enhance the difference in growth rates of different sized seed nanocrystals, i.e., to increase the ratio of the growth rate of the larger crystals to that of smaller ones—by tuning temperatures. According to eq 1, this may be achieved by decreasing the growth temperature, because the difference in supersaturation due to the size effect may become more significant with decreased temperature. On the basis of this understanding, we have designed a two-stage process for growth of ZnO nanowires, i.e., to divide the growth process into two stages at two different temperatures—the first stage at 88–89 °C for 10 min and the second stage at 85–86 °C for the desired amount of time. The idea is to allow the larger seed crystals to grow into large enough wires in the first stage so that lowering the temperature in the second stage will affect the growth of these wires much less significantly than it does to those smaller crystals. This idea was tested by experiments, and it was observed that lowering the temperature by 3 °C after the initial stage (~10 min) made the smaller crystals grow much slower or even dissolve due to Ostwald ripening (smaller crystals or sol particles dissolve and redeposit onto larger ones), while having a negligible effect on the growth rate of the wires that had already been grown during the first stage.

Our second approach is to reduce the zinc nitrate concentration in the chemical bath from the previously used 25 mM to 7.5 mM. As a result, mass transport becomes a limiting factor for growth of short wires as well as the lateral growth of long wires, especially at the root. By reducing the Zn^{2+} concentration, the Zn^{2+} may be depleted at the bottom of the wire array as the wires grow long, and therefore, growth of short wires as well as the radial growth of the long wires at the bottom of the array can be suppressed.

Figure 3 shows an array of 21–22 μm long ZnO nanowires synthesized by the process revised according to the above two

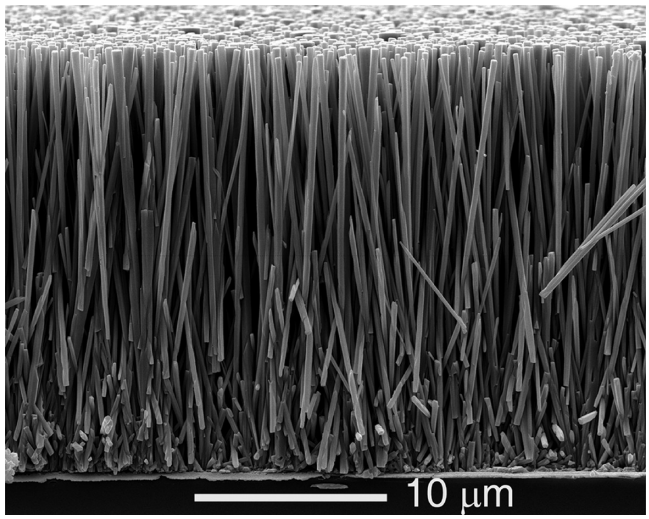

Figure 3. SEM images of ZnO nanowire arrays synthesized using the two-stage process developed in this paper. The growth solution bath consists of 7.5 mM $Zn(NO_3)_2$ + 3.75 mM HMTA + 0.15 M NH_4OH + 2 mM PEI. The bath temperature is kept at 88 °C for the first 10 min and then at 85 °C for 12 h.

approaches. The array has a high wire density (~8.3×10^8/cm^2) and high aspect ratio (~80). The average diameter of the wires is about 230 nm at the upper portion and about 280 nm at the lower portion, which is very thin for more than 20 μm long wires. Most importantly, the wires in Figure 3 remain separated with each other at the root, which is in clear contrast to the wires shown in Figure 1 as well as those shown in Figure 2a and b which are fused at the lower portion. Thus, the two-stage growth process, coupled with the use of less concentrated zinc nitrate, effectively avoids fusion of wires at their root and allows us to grow much longer wires than what we previously can without fusing the root.

Conversion of ZnO Nanowires into TiO_2 Nanotubes and DSCs Based on TiO_2 Nanotubes. Previous studies from our own and other groups have shown that DSCs based on TiO_2 nanowires or nanotubes generally perform better than those based on ZnO nanowires,[10,23,24] possibly due to surface chemical reactions,[25,26] formation of dye aggregates[26] and surface trap states[27] on the ZnO nanowires, and slow charge

dx.doi.org/10.1021/jp300960r | J. Phys. Chem. C 2012, 116, 7236–7241

injection from commonly used dyes to ZnO.[28] Therefore, in order to fabricate DSCs with better performance, we subsequently converted the resulting ZnO nanowire arrays, shown in Figure 3, into a TiO_2 nanotube array by following our previously published method.[10] Because the ZnO wires are not fused together at the root, the whole length of ZnO nanowires is accessible to the TiO_2 deposition solution and can be converted into TiO_2 tubes. The side-view and top-view SEM images and a transmission electron microscopy (TEM) image of the TiO_2 nanotube arrays with an open top-end are shown in Figure 4a, b, and c, respectively. The tubes have a hollow core

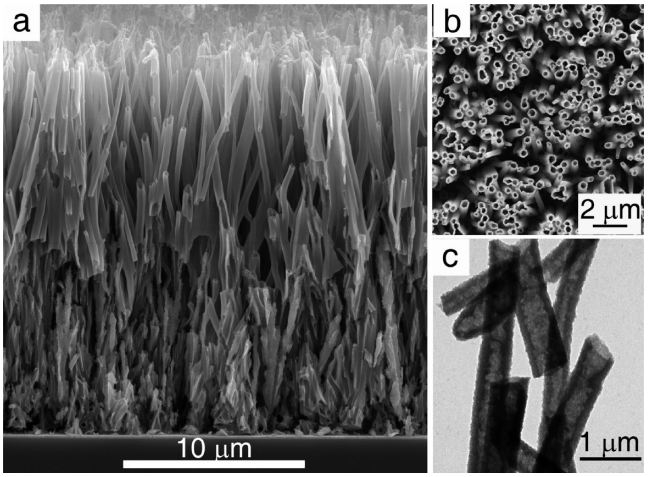

Figure 4. TiO_2 nanotube arrays converted from ZnO nanowire arrays: (a) side-view SEM image; (b) top-view SEM image of the TiO_2 nanotube arrays, showing the open tubes at the top-end; (c) TEM image of TiO_2 nanotubes.

and an about 30–50 nm thick wall. X-ray diffraction (XRD) pattern in Figure 5a indicates that the as-synthesized nanotubes consist of crystals of anatase TiO_2 and no crystalline ZnO is detected. In Figure 5b, the high-resolution TEM image of TiO_2 tubes shows that the tube wall is nonporous, dense, and of high crystallinity.

We synthesized arrays of ZnO nanowires in three lengths (10, 15, and 20 μm), converted them into top-end opened TiO_2 nanotube arrays, and fabricated DSCs with them. Current density–voltage (J–V) characteristics of these DSCs are shown in Figure 6a. The short circuit current (J_{sc}), open circuit voltage (V_{oc}), fill factor (FF), and power conversion efficiency (η) of these cells are summarized in Table 3. Corresponding increase in J_{sc} and η is observed as the film thickness increases. This apparently is the result of the increased internal surface area of the TiO_2 nanotube arrays. It is important to note that the efficiency of 6.1% for the DSC with 20 μm long TiO_2 tubes is significantly higher than most of the reported DSCs based on ordered structured anodes,[3−6,8,10,11] which can be attributed to the high internal surface area of the 20 μm thick TiO_2 nanotube array. Furthermore, this efficiency is close to that of 10 μm thick TiO_2 nanoparticle film-based DSCs reported in many publications, indicating a great potential of the present route in fabricating TiO_2 nanotube based DSCs.

The incident photon conversion efficiencies (IPCE) of these cells are shown in Figure 6b. The IPCE of TiO_2 nanotube-based DSCs shows a sustained increase as the film thickness increases to as thick as 20 μm, suggesting a high electron collecting efficiency of vertically aligned TiO_2 nanotubes. The

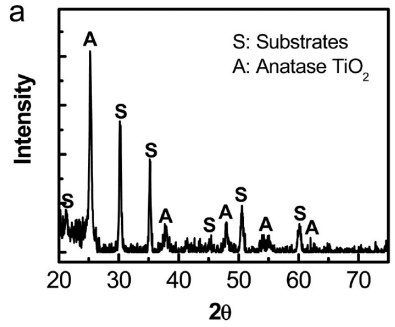

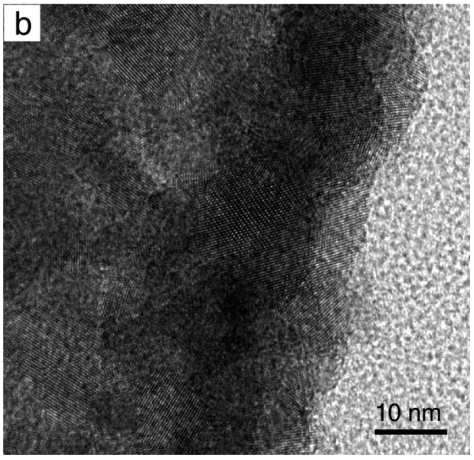

Figure 5. (a) XRD patterns of TiO_2 nanotube arrays. (b) High-resolution TEM image of the TiO_2 nanotube wall.

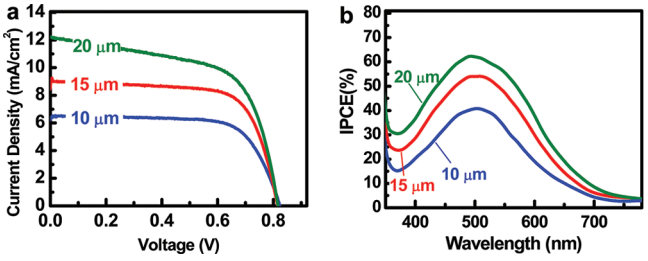

Figure 6. Photovoltaic performance of DSCs based on arrays of TiO_2 nanotubes in varied lengths: (a) current density–voltage (J–V) characteristics; (b) incident photon conversion efficiencies (IPCE).

Table 3. Photovoltaic Performance Data for TiO_2 Nanotube-Based DSCs with Sensitized Films in Varied Thicknesses

film thickness (μm)	J_{sc} (mA/cm^2)	V_{oc} (V)	FF	η (%)
10	6.5	0.825	0.703	3.8
15	9.2	0.814	0.685	5.2
20	12.2	0.816	0.613	6.1

efficient electron collection of TiO_2 nanotube-based DSCs can be attributed to the straight electron transport pathway in the vertically ordered TiO_2 nanotubes with a dense structure. The high electron collection efficiency suggests that there is still much room to further increase the efficiency of such DSCs by growing longer ZnO nanowires. It also opens up numerous opportunities to further improve DSCs, for example, by employing solid-state electrolytes and by using redox mediators with faster kinetics.

dx.doi.org/10.1021/jp300960r | J. Phys. Chem. C 2012, 116, 7236–7241

CONCLUSION

In summary, we have investigated the dependence of wire density and aspect ratio on the process parameters for synthesis of ZnO nanowire arrays and identified the major causes for fusion of wires at their root. On the basis of such studies, we have developed a two-step hydrothermal process for synthesis of long and ordered ZnO nanowire arrays directly on TCO. Compared with previously published methods, better control on the ZnO nanowire growth is gained through two approaches: (i) dividing the hydrothermal process into two steps at two different temperatures and (ii) reducing the Zn^{2+} concentration. The first approach enhances the growth rate difference between crystals in different sizes, so that, by lowering the growth temperature in the second step, the growth of those smaller seed crystals is effectively suppressed while the growth rate of those larger seed crystals that have grown into wires during the first step is not significantly affected. The second approach uses mass transfer limitation to suppress the lateral growth of wires as well as growth of short wires at the bottom of the nanowire array. By using this process, arrays of ZnO nanowires as long as 20 μm can be obtained with separated roots at the bottom of the arrays. Such ZnO nanowires can be converted to TiO_2 nanotubes which can be used as anodes in the fabrication of efficient DSCs. These DSCs yield power conversion efficiencies of up to 6.1%, which is significantly higher than most of the reported DSCs based on ordered structured anodes. This efficiency is also close to that of 10 μm thick TiO_2 nanoparticle film based DSCs reported in many publications, indicating a great potential of the present route in fabricating TiO_2 nanotube-based DSCs. The IPCE of these cells suggests that the electron collection of the TiO_2 nanotube-based anodes is highly efficient, which opens up numerous opportunities to further improve DSCs, for example, by employing solid-state electrolytes and by using redox mediators with faster kinetics.

AUTHOR INFORMATION

Corresponding Author

*E-mail: gaod@pitt.edu.

Notes

The authors declare no competing financial interest.

ACKNOWLEDGMENTS

This work was supported by the National Science Foundation (grant CBET 0967722).

REFERENCES

(1) Michael, G. *J. Photochem. Photobiol., C* **2003**, *4*, 145.
(2) Martinson, A. B. F.; Hamann, T. W.; Pellin, M. J.; Hupp, J. T. *Chem.—Eur. J.* **2008**, *14*, 4458.
(3) Baxter, J. B.; Aydil, E. S. *Appl. Phys. Lett.* **2005**, *86*, 053114.
(4) Law, M.; Greene, L. E.; Johnson, J. C.; Saykally, R.; Yang, P. *Nat. Mater.* **2005**, *4*, 455.
(5) Baxter, J. B.; Walker, A. M.; Ommering, K. v.; Aydil, E. S. *Nanotechnology* **2006**, *17*, S304.
(6) Mor, G. K.; Shankar, K.; Paulose, M.; Varghese, O. K.; Grimes, C. A. *Nano Lett.* **2006**, *6*, 215.
(7) Feng, X.; Shankar, K.; Varghese, O. K.; Paulose, M.; Latempa, T. J.; Grimes, C. A. *Nano Lett.* **2008**, *8*, 3781.
(8) Liu, B.; Aydil, E. S. *J. Am. Chem. Soc.* **2009**, *131*, 3985.
(9) Varghese, O. K.; Paulose, M.; Grimes, C. A. *Nat. Nano* **2009**, *4*, 592.
(10) Xu, C.; Shin, P. H.; Cao, L.; Wu, J.; Gao, D. *Chem. Mater.* **2010**, *22*, 143.
(11) Xu, C.; Shin, P.; Cao, L.; Gao, D. *J. Phys. Chem. C* **2010**, *114*, 125.
(12) Wang, J.; Lin, Z. *Chem. Mater.* **2008**, *20*, 1257.
(13) Galoppini, E.; Rochford, J.; Chen, H.; Saraf, G.; Lu, Y.; Hagfeldt, A.; Boschloo, G. *J. Phys. Chem. B* **2006**, *110*, 16159.
(14) Martinson, A. B. F.; McGarrah, J. E.; Parpia, M. O. K.; Hupp, J. T. *Phys. Chem. Chem. Phys.* **2006**, *8*, 4655.
(15) Jennings, J. R.; Ghicov, A.; Peter, L. M.; Schmuki, P.; Walker, A. B. *J. Am. Chem. Soc.* **2008**, *130*, 13364.
(16) Martinson, A. B. F.; Góes, M. r. S.; Fabregat-Santiago, F.; Bisquert, J.; Pellin, M. J.; Hupp, J. T. *J. Phys. Chem. A* **2009**, *113*, 4015.
(17) Xin, X.; Wang, J.; Han, W.; Ye, M.; Lin, Z. *Nanoscale* **2012**, *4*, 964.
(18) Xu, C.; Wu, J.; Desai, U. V.; Gao, D. *J. Am. Chem. Soc.* **2011**, *133*, 8122.
(19) Wang, J.; Zhao, L.; Lin, V. S. Y.; Lin, Z. *J. Mater. Chem.* **2009**, *19*, 3682.
(20) Wang, J.; Lin, Z. *J. Phys. Chem. C* **2009**, *113*, 4026.
(21) Greene, L. E.; Law, M.; Tan, D. H.; Montano, M.; Goldberger, J.; Somorjai, G.; Yang, P. *Nano Lett.* **2005**, *5*, 1231.
(22) Sangwal, K. In *Additives and Crystallization Processes*; John Wiley & Sons, Ltd: Hoboken, NJ, 2007; p 265.
(23) Wang, J.; Lin, Z. *Chem. Mater.* **2009**, *22*, 579.
(24) Ye, M.; Xin, X.; Lin, C.; Lin, Z. *Nano Lett.* **2011**, *11*, 3214.
(25) Horiuchi, H.; Katoh, R.; Hara, K.; Yanagida, M.; Murata, S.; Arakawa, H.; Tachiya, M. *J. Phys. Chem. B* **2003**, *107*, 2570.
(26) Oekermann, T.; Yoshida, T.; Minoura, H.; Wijayantha, K. G. U.; Peter, L. M. *J. Phys. Chem. B* **2004**, *108*, 8364.
(27) Goldberger, J.; Sirbuly, D. J.; Law, M.; Yang, P. *J. Phys. Chem. B* **2004**, *109*, 9.
(28) Wu, J.-J.; Chen, G.-R.; Yang, H.-H.; Ku, C.-H.; Lai, J.-Y. *Appl. Phys. Lett.* **2007**, *90*, 213109.